Induced martensitic transformation during tensile test in nanostructured bainitic steels

L. Morales-Rivas[1,2], C. Garcia-Mateo[1]*, Matthias Kuntz[3], Thomas Sourmail[4], F.G. Caballero[1]

[1]Department of Physical Metallurgy, National Center for Metallurgical Research (CENIM-CSIC). Avda. Gregorio del Amo, 8, 28040, Madrid, Spain.

[2]University of Kaiserslautern, Materials Testing, Gottlieb - Daimler - Str., 67663, Kaiserslautern, Germany.

[3]Robert Bosch GmbH, Materials and Processing Dept, P.O. Box 300240, Stuttgart, Germany.

[4]Asco Industries CREAS (Research Centre) Metallurgy, BP 70045, Hagondange Cedex 57301, France.

*Corresponding author: Carlos Garcia-Mateo. cgm@cenim.csic.es. Tf: +34 91 5538900 Fax: 34 91 534 74 25. National Centre for Metallurgical Research (CENIM-CSIC). Avda. Gregorio del Amo 8. Madrid E-28040. Spain.

1- ABSTRACT

Retained austenite in nanostructured bainite is able to undergo mechanically induced martensitic transformation. However, the link between transformation and deformation mechanisms involved makes difficult the understanding of the process. In this work, a model has been developed to assess the effect of the external stress itself on the martensite phase transformation. In addition, after a detailed initial microstructural characterization, the martensite fraction evolution during tensile deformation has been obtained by means of X-ray diffraction analyses after interrupted tensile tests in several nanostructured bainitic steels. Experimental results have been compared to the outputs of the model, as a reference. They suggests that stress partitioning between phases upon tensile deformation is promoted by isothermal transformation at lower temperatures.

2- INTRODUCTION

TRIP-assisted multiphase steels are advanced microstructures which present an improved balance of strength and ductility thanks to the so-called TRIP-effect, i.e. transformation induced plasticity (TRIP) of the retained austenite into martensite. These microstructures normally consist of a soft matrix of allotriomorphic ferrite and a dispersed microconstituent, e.g., bainite, consisting of bainitic ferrite plus retained austenite [1]. Apart from the TRIP effect, other mechanisms are involved in these steels during

tensile deformation, including the well-known Hall-Petch strengthening mechanism, and also the composite-type of strengthening plays a big role. The coupling between plasticity and the mechanically induced transformation is thus complex, often without a clear distinction between cause and effect [2]. There is a strong relation between strain hardening and TRIP effect, but it is difficult to know the extent at which the austenite evolution occurs as a consequence of the stress-strain behavior, and how this transformation affects the work hardening mode in return. Two different martensitic transformation mechanisms have been reported in TRIP steels: stress-assisted and strain-assisted TRIP effect. In the first situation, stress-assisted, martensitic nucleation takes place on the same heterogeneous sites responsible for the transformation on cooling. In this case, kinetics of transformation governs kinetics of macroscopic deformation. However, in the other case, strain-assisted TRIP effect, martensitic transformation takes place thanks to the new nucleation sites being created, shear-band intersections; that is, prior plastic strain is necessary to trigger TRIP under this condition. Regardless of the TRIP mode, stress- or strain-assisted, the presence of an external mechanical stress has an effect on the total driving force for martensitic transformation, $|\Delta G^{\gamma-\alpha'}|$, which must include a mechanical term, ΔG_{mech}, dependant on that stress [6, 3]. There is some controversy on whether martensitic transformation occurs either by a stress-assisted or by a strain assisted mode depending on the microstructure [3].Recently, many works on TRIP-assisted steels have been devoted to develop constitutive models, normally based on finite element analyses multiscale simulations, for the formulation of the flow strength of the evolving multi-phase composite. For this purpose, the knowledge of the transformation kinetics law describing the evolution of the volume fraction of austenite is compulsory, which is addressed by implementing different models [4, 5, 6, 7, 8, 9]. The complexity arises from the fact that the stability of the retained austenite depends on many factors, as its chemical composition, morphology and size. A low stability for retained austenite can be ascribed to its low carbon content as well as to a relatively large grain size [10]. Moreover, stability is highly affected by the relative mechanical properties of the austenite and the surrounding phases, and the corresponding stress partitioning between them [5, 11, 12, 13].

In this work, a set of microstructures belonging to a new generation of steels, nanostructured bainite, have been studied. The presence of retained austenite and the occurrence of TRIP effect in these microstructures is well-known [14, 15]. However, the major phase of these nanostructured steels is not allotriomorphic ferrite, as in conventional TRIP-assisted steels, which is absent, but bainitic ferrite. Bainitic ferrite presents, instead, a high strength due to its nanometric size, a high dislocation content,

and the tetragonality associated to its C supersaturation [16, 17, 18]. Thus, the deformation mechanisms of these microstructures are thought to differ from those of the conventional TRIP-assisted steels.

It is not the purpose of this work to design a constitutive model for nanostructured bainite. Instead, a model will be implemented to isolate and assess the effect that mechanical stress alone has on the martensitic transformation start temperature, M_s, and thus, on the martensitic transformation evolution.

3- MATERIALS AND EXPERIMENTAL PROCEDURE

A total of three steels have been used for this work, and their chemical compositions are given in Table 1. The heat treatment consisted in a first stage of austenitization, a subsequently cooling down to a temperature between the bainitic start temperature (B_s) and the martensitic start temperature (M_s), an isothermal holding at that temperature for the bainitic transformation, and finally an accelerated cooling down to room temperature. As shown in Table 2, for each steel two isothermal temperatures were selected to assess differences in the nanostructured bainite features and its performance.

Tensile tests were performed at room temperature in specimens of 8 mm diameter and 20 mm of gauge length at a deformation rate of 0.004 s^{-1}. The load-displacement data during tests was obtained from an extensometer fitted to electronic equipment. Apart from tensile tests performed until fracture, some tensile tests were intentionally interrupted at the uniform deformation region in order to track the austenite fraction evolution. For that purpose, selected cross-sections of the gauge length, perpendicular to tensile direction, were extracted.

Table 1 Chemical composition of the studied steels.

	Chemical composition [wt.%]								
	C	Si	Mn	Ni	Mo	Cr	V	Cu	Al
Steel 1	1.0	1.50	0.74	0.12	0.03	0.97	0.00	0.17	0.025

Steel 2	0.6	1.67	1.32	0.20	0.15	1.73	0.12	0.18	0.03
Steel 3	0.6	2.5	1.32	0.20	0.15	1.73	0.12	0.18	0.03

Table 2. Heat treatment settings of the studied samples.

	Samples	Bainitic transformation	
		Temperature [˚C]	Time [h]
Steel 1	1C1.5Si_250	250	16
	1C1.5Si_220	220	16
Steel 2	0.6C1.5Si_250	250	16
	0.6C1.5Si_220	220	22
Steel 3	0.6C2.5Si_250	250	16
	0.6C2.5Si_220	220	24

The microstructure was observed by secondary electron scanning electron microscopy (SE-SEM). Metallographic samples were cut, ground and polished following the standard procedures, including a final step of polishing with colloidal silica suspension. A 2% Nital etching solution was used to reveal the phases. Scanning electron microscopy (SEM) observation was carried out on a JEOL JSM-6500F field emission gun scanning electron microscope (SEM-FEG) operating at 10 kV.

The determination of the fraction of retained austenite (VF_γ) of undeformed and deformed samples was achieved by means of X-ray diffraction (XRD) analyses. Specimens were prepared by a standard grinding and polishing procedure, finishing with a step of polishing with 1 μm diamond paste. Several cycles of etching and polishing were applied in order to remove the deformed layer. XRD measurements were performed with a Bruker AXS D8 diffractometer equipped with a Co X-ray tube, Goebel mirror optics and a LynxEye Linear Position Sensitive Detector for ultra-fast XRD measurements. A current of 30 mA and a voltage of 40 kV were employed as tube settings. Operational conditions were a 2θ range of 35 -135˚ and a step size of 0.01˚. The volume fraction of the retained austenite was calculated from the integrated intensities of (111), (002), (022) and (113) austenite peaks, and those of (011), (002) and

(112) planes of ferrite, with the equation for the ratio of these experimental values to the normalization factors for peaks intensity (R) given in the ASTM E975-08 [19]. More details on the XRD experimental procedure can be found in ref. [16].

All the necessary thermodynamics calculations were performed using MtData in combination with the SGSOL-SGTE Solution database [20]. Crystallographic simulations have been coded using the free and open-source MTEX toolbox [21] running in MATLAB [22].

4- RESULTS AND DISCUSSION

Initial microstructure

For all heat treatments the microstructure consists of a mixture of two phases, bainitic ferrite and retained austenite. The addition of Si avoids the massive carbide precipitation [23]. Further details on the characterization of these microstructures can be found elsewhere [18, 24, 25]. Fig.1(a) and Fig.1(b) show scanning electron micrographs of the microstructures corresponding to samples 1C1.5Si_250 and 1C1.5Si_220, respectively. The etched phase corresponds to bainitic ferrite plates and the higher relief to retained austenite, this latter present in two different morphologies, as films (γ_f) and as blocks (γ_b), Fig.1. Due to the nature of the bainitic transformation and geometrical restrictions of the mentioned austenite features, films of austenite are more enriched in C in solid solution than blocks of austenite [10]. In these microstructures, C does not only lay at defect-free solid solution but also at defects such as twin and phase boundaries, clusters or dislocations [18, 26].

The initial fractions of austenite, $VF_{\gamma 0}$, are summarized in Table 3. Considering each steel, for Steel 2 and Steel 3, the initial volume fraction of austenite is similar in both samples regardless of the treatment temperature. However, for Steel 1, $VF_{\gamma 0}$ is considerably higher in the sample treated at lower temperature, 1C1.5Si_220, than in 1C1.5Si_250. This is due to an isothermal treatment time insufficient for the completion of the bainitic reaction in the case of 1C1.5Si_220.

Mechanical properties

Table 3 gathers the results from tensile tests. YS increases as the treatment temperature does. In nanostructured bainitic steels, YS has been proven to depend mainly on the volume fraction of the phases and the scale of bainitic ferrite [27]. In this sense, a high fraction of slender bainitic ferrite plates usually results in a high YS [28]. Attending to YS values in Table 3, the refinement of the microstructure

which takes place at lower temperatures does not imply an increase of YS. It is clear that another factor contributing to YS is the austenite strength, i.e., its C content [29], which must be thus playing a role. It has been recently reported that at high transformation temperatures there is an extra C enrichment of austenite, as C trapped at defects, boundaries and forming clusters is favored to partition into austenite defect-free solid solution [18]. Therefore, considering each steel, even for samples having the same phase volume fraction regardless of the treatment temperature, austenite is expected to have a higher C content in the cases of samples treated at 250˚C.

Table 3. Initial fraction of austenite ($VF_{\gamma 0}$), yield strength (YS), ultimate tensile strength (UTS), uniform elongation (UE), true stress at martensitic transformation start ($\sigma_{\gamma\text{-}\alpha'}$) and its corresponding true plastic deformation ($\varepsilon_{\gamma\text{-}\alpha}$) measured according to description in the main body of the text.

	$VF_{\gamma 0}$ [%]	YS [MPa]	UTS [MPa]	UE [%]	$\sigma_{\gamma\text{-}\alpha'}$ [MPa]	$\varepsilon_{\gamma\text{-}\alpha}$ [%]
1C1.5Si_250	33± 3	1731±17	2172±5	8.8±0.5	2018	0.9
1C1.5Si_220	39± 3	1161±49	2063±60	3.0±0.4	1604	0.9
0.6C1.5Si_250	18± 3	1435±24	1990±2	8.2±0.2	1636	0.5
0.6C1.5Si_220	22± 3	1241±15	2127±154	4.6±2.6	1164	-
0.6C2.5Si_250	24± 3	1467±13	1950±11	8.1±2.3	1556	0.3
0.6C2.5Si_220	23± 3	1350±24	2037±18	3.0±0.1	1408	0.3

In Fig.2, experimentally obtained martensite fractions, defined as ($VF_{\gamma 0}$-VF_{γ}), are plotted vs. ln (true stress), where VF_{γ} is the fraction of austenite for different levels of deformation, measured after interrupted tensile tests. Their corresponding linear regression analyses are also plotted, Fig.2, from which the true stress at which martensitic transformation starts, $\sigma_{\gamma\text{-}\alpha'}$, is estimated, Table 3. Their corresponding values of true plastic strain at which martensitic transformation starts, $\varepsilon_{\gamma\text{-}\alpha}$, have been calculated interpolating $\sigma_{\gamma\text{-}\alpha'}$ in the corresponding true stress-true plastic strain curve.

In all cases but 0.6C1.5Si_220, martensitic transformation starts after the macroyielding of the microstructure, i.e., over the YS. Therefore, one or both phases, bainitic ferrite and austenite, have

started to yield before TRIP effect takes place. Only for 0.6C1.5Si_220 the stress at the yielding onset is slightly lower than the macroscopic yielding stress, and thus, plastic strain at that point cannot be reported. It is necessary to highlight that for this condition, lack of data at the first stages of the transformation could have led to an underestimation of the $\sigma_{\gamma-\alpha'}$ value; note that the first point for the fitting corresponds to a martensite fraction of 7%, whereas in the other cases is about 2-3%.

When representing martensite evolution as a function of plastic strain, Fig. 3, it is clear that transformation tend to be more progressive in samples treated at higher temperatures, in good agreement with results reported in previous works [14, 30]. In this same figure, the critical strain necessary for the mechanical stabilization of austenite, ε_c, is represented as vertical dotted lines. The mechanical stabilization accounts for the generation, during straining and transformation, of new dislocations that impede the phase transformation of austenite into martensite. It is well known [31, 32, 33, 34] that when the strain in the austenite becomes sufficiently large, reaching the mentioned critical value, ε_c, the motion of the glissile interfaces is not possible anymore, causing the transformation to halt. ε_c can be calculated according to Chatterjee et al. [35].

Two different values of the critical strain, Fig. 3, are represented and denoted as min. and max. The former corresponds to the value of ε_c assuming that as explained, due to geometrical restrictions, the austenite submicron blocks hardly enrich in C. Therefore, a size of 1 μm and a C content equal to that of the bulk composition is imposed for the calculation of the min. value in Fig. 3. On the other hand, the max. value of ε_c has been calculated assuming that the thin films of retained austenite, 50 nm thick, are enriched in C to the level of 2 times the bulk C content, i.e. 2 wt. % for Steel 1, and 1.2 wt.% for Steel 2 and Steel 3, as reported by Atom Probe Tomography measurements in similar microstructures with similar initial fractions of retained austenite [10]. However, in all cases the overall martensitic transformation seems to still take place beyond the maximum critical strain values. If it is the case of strain-induced martensitic transformation, plastic strain in austenite can avoid mechanical stabilization by the favouring of variants which grow across slip planes [36, 37]. The possibility that strain is indeed ruling the martensitic transformation will be considered by the application of existing models of strain-assisted martensitic transformation. Such models, originally developed for homogeneous austenitic alloys to calculate the volume fraction of strain-induced martensite, have been reviewed and applied to TRIP steels by Samek et al. [38]. There are two reported kind of dependences between the formed martensite fraction and the plastic strain. One of them can be described by the Burke–Matsumura–Tsuchida (BMT) equation [39, 40, 41]:

$$VF_{\alpha'} = \frac{VF_{\gamma 0}}{1+\frac{p}{k_p.\varepsilon^p.VF_{\gamma 0}}} \qquad \text{eq. 1}$$

where $VF_{\alpha'}$ stands for the current formed martensite fraction; $VF_{\gamma 0}$, for the initial austenite fraction; ε, the plastic strain; p is the autocatalytic strain exponent; and k_p.is a constant related to the austenite stability.

The other one can be represented by the Guimarães equation [42], which is equivalent to the well known formula by Olson and Cohen [38, 43]

$$VF_{\alpha'} = VF_{\gamma 0}\left(1 - e^{-k_G.\varepsilon^z}\right) \qquad \text{eq. 2}$$

where z and k_G are fitting parameters.

After obtaining the appropriate parameters for linearization, fittings with BMT equation and Guimarães equation are shown in Fig. 4 a and b, respectively, where the parameter true plastic strain replaces ε. In the first case, BMT model, p is assumed to be 1 for simplicity, meaning that the autocatalysis is a negligible transformation mechanism. The values of k_p. obtained by fitting by least squares fitting are listed in Table 4 For each alloy, the lowest values of k_p. correspond to samples treated at the highest temperature, which is consistent with the higher stability of austenite in that case, which tends to be more enriched in C [18]. In the case of Guimarães fitting, the trend lines for the different samples do not converge at a ε (true plastic strain) of 1 (i.e., Ln(ε)=0), implying that k_G is not constant (Table 4). The apparent higher k_G values for samples treated at lower temperatures might be consequence of the lower austenite stability, but it might be hiding a probable strain partitioning phenomenon between the phases. The actual composite conditions are likely neither equal strain nor equal stress between the phases, but an intermediate situation, where the softer phase presents lower stress and higher strain than the composite mean values [44]. Thus, austenite of samples treated at 220°C might be in fact the softest phase for low transformation temperatures, subjected to a higher strain than the macroscopic value, the true plastic strain, with respect to samples treated at 250°C. On the other hand, the slopes of the trend lines are also different (z in Table 4). A value of z = 2 corresponds to a random orientation of the shear-band intersections. In general shear bands will not be initially randomly oriented and will tend to be parallel until secondary shear systems begin to operate, a behavior that can be depicted by an

exponent higher than z=2 [43]. It cannot be physically explained the fact that fitted values of z in Table 4 are mostly lower than 2. Therefore the Guimarães model has a limited applicability in this case.

Table 4. Fitting parameters of the strain-induced martensitic transformation models.

	BMT fitting	Guimarães fitting	
	$k_{p.}$	k_G	Z
1C1.5Si_250	17.76	7.5	1.15
1C1.5Si_220	19.12	331.7	2.03
0.6C1.5Si_250	77.38	3.7	0.66
0.6C1.5Si_220	231.91	9.4	0.68
0.6C2.5Si_250	4.17	2.5	0.66
0.6C2.5Si_220	88.01	19.0	1.03

Regardless of the goodness of fitting of the strain-assisted models, it might be in same cases fortuitous, as indicated by Chatterjee and Bhadeshia [3]. Effects associated to strain-assisted transformation become prominent at large strains but at low plastic strains they can be negligible. For example, in fully austenitic steels, martensitic transformation can be modelled as stress-assisted even beyond austenite yield strength, at strains up to 10% [45]. Therefore, the applied stress may have also itself an important influence by increasing the driving force for the martensitic transformation.

The isolated effect of the applied stress will be assessed from now on through a model for austenite evolution as a function of the overall true stress, considering no stress partitioning condition and stress-assisted transformation, among others. The implications of such assumptions will be discussed.

Simplified model for stress-assisted martensitic transformation in nanostructured bainite.

The evolution of texture as a consequence of the mechanically-induced martensitic transformation has been modeled in fully austenitic steels so that crystallography can be correctly predicted [45]. However, the relationship between the interaction energy and fraction transformed is not so clear [45]. In nanostructured bainite, in turn, texture does not only depend on the martensitic transformation, but also on the way how microstructure deforms plastically [30].

Chatterjee et al. [3], proposed that, when stress-assisted conditions are fulfilled, the austenite volume fraction evolution during tensile testing can be calculated as a function of (M_s –T), using the equation of a thermal martensitic transformation on quenching by Koistinen-Marburger [46]:

$$VF_{\alpha'} = VF_{\gamma 0}\left(1 - e^{-0.011(\mathrm{M_s}-\mathrm{T})}\right) \qquad \text{eq. 3}$$

where $VF_{\alpha'}$ stands for the current formed martensite fraction; $VF_{\gamma 0}$, for the initial austenite fraction; M_s, for the martensitic start temperature; and T, for the test temperature. In the case of transformation on quenching, T changes and M_s keeps constant, whereas in the case of Chatterjee's model, M_s changes as a function of the applied stress and T is the constant room temperature.

The M_s is obtained as the temperature at which $|\Delta G^{\gamma-\alpha'}|$ = ΔG_{crit} , where ΔG_{crit} is the critical driving force needed to stimulate martensite by an athermal diffusionless nucleation and growth mechanism [47]. In Chatterjee's work, a new term is added to $|\Delta G^{\gamma-\alpha'}|$, the ΔG_{mech} , that, for simplicity is calculated assuming the most favourably oriented austenite crystal. Although based in Chatterjee's work, the novelty of the present work resides in the fact that it accounts for the polycrystalline nature of retained austenite. In addition, and similarly as proposed by Lani et al [4], in this work, the term ΔG_{crit} incorporates all the unknowns regarding the plastic and elastic accommodation work, which, for simplicity, is required to be constant upon deformation, and obtained for every sample as follows: after an iterative process, ΔG_{crit} is set to a value such that the simulated martensitic transformation begins at the empirically obtained $\sigma_{\gamma\text{-}\alpha'}$ (Table 3) value.

A total of 2000 prior austenite random orientations have been simulated. All grains are considered to have an initial austenite fraction of 1/2000 and an austenite unique C content. Each austenite grain is considered to hold at the beginning 4 potential habit planes belonging to the family {1 1 1}. The plane {1 1 1} is reported to be the habit plane in low-alloy steels [48]. Then, $|\Delta G^{\gamma-\alpha'}|$ is calculated for each habit plane of each austenite grain as a sum of two terms: the chemical driving force, ΔG_{chem}; and the

mechanical driving force, $\Delta G_{mech} = \sigma_n \delta + \tau s$, where σ_n stands for the normal component of the applied tensile stress on the martensite habit plane; τ for the shear component of the applied stress, parallel to the habit plane; and δ and s, the dilatational and shear strains, 0.163 J/(mol·MPa) and 1.551 J/(mol·MPa), respectively. Therefore, ΔG_{mech}on a habit plane which holds an angle θ with the tensile direction, at a tensile stress σ, is approximated as eq. 4 [49]:

$$\Delta G_{\mathrm{mech}} = \frac{1}{2} s\, \sigma \sin(2\theta) + \frac{1}{2} \delta\sigma\, (1 + \cos(2\theta)) \qquad \text{eq. 4}$$

Therefore it is possible to calculate a M_s temperature for each habit plane, as already described.

For every prior austenite grain, *i*, only the highest $M_{s,}$ out of the four potential M_s values is considered to calculate its martensite fraction, provided that the value is higher than room temperature. The total fraction of martensite for a certain stress is, thus, calculated as the sum of martensite fraction in every simulated grain, i.e.:

$$VF_{\alpha'} = \sum_{i=1}^{2000} VF_{\gamma 0\mathrm{i}} \left(1 - e^{-0.011\left(M_{s\_max}(\mathrm{i}) - T\right)}\right) \qquad \text{eq. 5}$$

where *T* is the room temperature, 25°C; $M_{s\_max}(i)$, the highest M_s of the grain *i*, provided that ($M_{s\_max}(i)$-*T*) is a positive value; and $VF_{\gamma 0\mathrm{i}}$ the initial fraction of austenite per grain, 1/2000.

Application of the simplified model

The model described has been applied to all experiments in Table 2. The austenite C content, input for the model, is considered to be the average C content of austenite, which is assumed to range between a lower and an upper limit for each condition. The minimum value is set as the bulk average C content. The upper value of austenite C content is set as approx. 0.5 wt. % above the bulk mean C content, a value close to those reported in other nanostructured bainitic steels [14, 18].

Results of such simulation are plotted together with experimental data of austenite fraction evolution. Attending the simulated curves, it is important to note first the subtle differences between those for upper and lower austenite C content, dotted lines in Fig.5. It can be stated thus that the average C content makes no difference in the martensite fraction evolution as a function of the stress increment. It is proven that retained austenite tends to be more enriched in C as the treatment temperature increases, even for the expected cases in which the volume fraction of austenite remaining after higher treatment temperatures is higher than the one left after lower treatment temperatures [18]. Even

though the average C content in austenite has been shown to have little contribution on the martensitic transformation evolution with respect to the stress increment, the C content of austenite highly affects its strength, which will be later discussed.

When comparing experimental and simulated data, Fig. 4, the simulated curves seem to establish an upper limit for the martensitic transformation. Therefore, assumption of stress-assisted martensitic transformation might be correct in those cases, since plastic deformation does not contributes to increase the martensitic transformation rate (with respect to the stress increment) above the expected rate predicted by the effect of the applied mechanical stress alone. Therefore, although plastic deformation is necessary to trigger or allow the phase transformation, transformation seems to occur assisted by the mechanical stress.

As opposed to the behaviour observed in Fig. 3, where samples treated at higher temperature showed a lower martensitic transformation rate as a function of the strain, the martensitic transformation rate as a function of stress is, for each steel, higher for samples treated at the highest temperature, 250˚C (experimental points in Fig.5). The reason is that in those samples, work-hardening is softer, in the sense that the slope of the stress-strain curve is lower, with respect to behaviour of samples treated at 220˚C.

The analysis can be approached in terms of the stress partitioning between the phases, as the average stress over austenite, σ_γ, may not necessarily be equal to the macroscopic true stress. The clearest example of differences in martensite evolution as a function of stress is in Steel 1. In sample 1C1.5Si_250 the fitting between the experimental and the simulated evolution of martensite fraction shows a good agreement. It suggests that the actual stress endured by austenite, $\sigma_{\gamma,}$ is, in that range, similar to the macroscopic true stress, so that stress is likely to partition equally between bainitic ferrite and austenite. It agrees with reported results from AFM-based nanoindentation on a microstructure obtained after isothermal treatment at 300^{o}C, where the yield strength of bainitic ferrite is similar to that of austenite [50]. However, for 1C1.5Si_220, the actual martensite fraction is lower than the simulated martensite fraction. It suggests that even though austenite is exposed to a gradually increasing σ_γ, this value is always lower than the macroscopic true stress. For 1C1.5Si_220, the macroscopic true stress would be 2.5 times the value of σ_γ. This is consistent with the possibility that in this case bainitic ferrite plus newly formed martensite are exerting a shielding effect over untransformed austenite, as reported in TRIP-assisted steels [51]. The lower average C content of retained austenite in samples treated at lower

temperatures is responsible for the drop in the strength of the austenite, phase which, in that case, must endure thus a lighter load than the surrounding bainitic ferrite and martensite [52].

Obviously, the ratio σ_γ/macroscopic true stress also depends on the fraction of the phases. However, for Steel 2 and Steel 3 the austenite fraction does not change as a function of the treatment temperature. Moreover, for Steel 1, in the sample treated at the lowest treatment temperature, 220° C, the volume fraction of austenite is even higher than for sample treated at 250° C. This higher fraction of austenite in 1C1.5Si_220 should contribute to equalise σ_γ and the macroscopic true stress, which is not observed. Therefore, as suggested, besides the phase fraction, the relative mechanical properties between the phases are ruling the observed behaviour. The sensitivity of the model results to some of the input parameters and the inclusion of new ones is discussed in the next section.

Variations of the model

The simulation has been repeated, but choosing this time the plane {2 5 9} as the habit plane, as reported for carbon steels with a C content of 1.8wt.% [48]. That C content is likely to be lower than the C content of small austenite features (films), especially in Steel 1, whose C content in bulk is 1wt.%. Results (an example in Fig. 6) reveal little differences in the theoretical evolution of austenite if the habit plane is changed. Only a slight higher rate of martensitic transformation with respect to the stress increment at the beginning. This is consequence of the lower sensitivity of the austenite stability to its crystal orientation when the habit plane is {2 5 9}, as compared to the habit plane {1 1 1}.

Finally, differences in martensite fraction evolution between samples treated at 220˚C and those treated at 250˚C cannot be due solely to the average C content, as explained, as there are other factors affecting the stability of austenite. It is important to emphasize the fact that heterogeneity in austenite features size/morphology, also associated to a heterogeneous C distribution has not been considered so far. Different austenite stabilities within a microstructure must result in different critical stresses at which transformation start. The critical stress at which blocks start to transform into martensite can be empirically obtained, according to the same experimental procedures followed in the algorithm of the simplified model. If we assume ΔG_{crit} to be constant for each sample regardless of the austenite feature considered (film or block), it is possible to theoretically determine the stress at which the austenite features most enriched in C (films) start to transform into martensite. In a new version of the algorithm, the presence of both block and films has been considered, with the following settings:

-Austenite blocks have the average C content.

-Austenite films have a C content which is 5 times the bulk content [18].

-The same volume fraction of austenite films and of austenite blocks is considered [15].

Besides these settings regarding the C content in austenite, the restrictions to martensitic transformation imposed by the austenite morphology are taken into account in this new algorithm:

-For austenite blocks, all the planes belonging to the family {1 1 1} can be active, from which the most favorably one is selected, as in the previous algorithm.

-For austenite films only one plane belonging to the family {1 1 1} can be active, which is randomly chosen.

This new model has been implemented on Steel 2 treated at both temperatures. Simulated curves of martensite evolution vs. stress show a higher resistance to martensitic transformation, as could be expected, Fig. 7. The experimental results are also explained by considering the heterogeneity in austenite. Moreover, the model predicts a kink point at the stress at which the transformation of films is triggered (at 2000 MPa for 0.6C1.5Si_250 and at 1600 MPa for 0.6C1.5Si_220), which might be also experimentally observed.

CONCLUSIONS

In nanostructured bainitic steels, plastic deformation prior to mechanically induced martensitic transformation is necessary. However, it does not rule out the possibility of stress-assisted mode of martensitic transformation. In fact, strain does not seem to promote transformation once it has already started. Stress partitioning between the phases depends on the heat treatment and the corresponding resulting initial nanostructured bainite. As samples are treated at higher treatment temperatures, the stress over austenite tends to the macroscopic stress value, due to the high C enrichment of the austenite, whereas as treatment temperatures decrease, there is a more significant shielding effect of banitic ferrite / martensite over the remaining retained austenite. The complexity of the microstructure, regarding the austenite morphology/size and C content distribution in austenite, makes the martensite fraction evolve at a lower rate as a function of the stress increment than it is predicted for homogeneous austenite. Therefore, the observed shielding effect over homogeneous austenite might overestimate the actual one.

5- ACKNOWLEDGEMENTS

The authors gratefully acknowledge the support of the European Research Fund for Coal and Steel, the Spanish Ministry of Economy and Competitiveness and the Fondo Europeo de Desarrollo Regional (FEDER) for partially funding this research under the contracts RFSR-CT-2012-00017, RFSR-CT-2014-00016 and MAT2013-47460-C5-1-P respectively. LM-R also acknowledges this same Ministry for financial support with ref. FPI : BES-2011-044186.

FIGURES

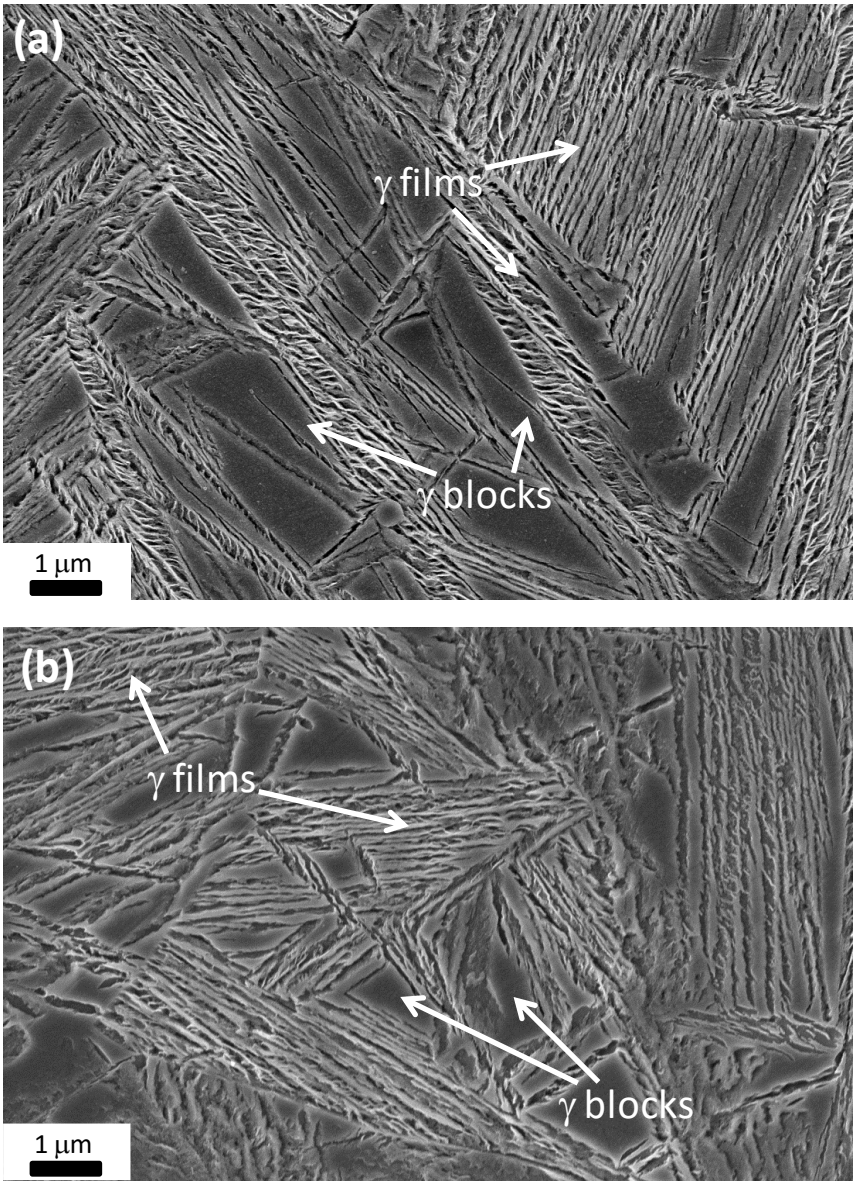

Fig.1. SEM image of: a) 1C1.5Si_250 and b) 1C1.5Si_220; where different austenite features, blocks and films, are indicated.

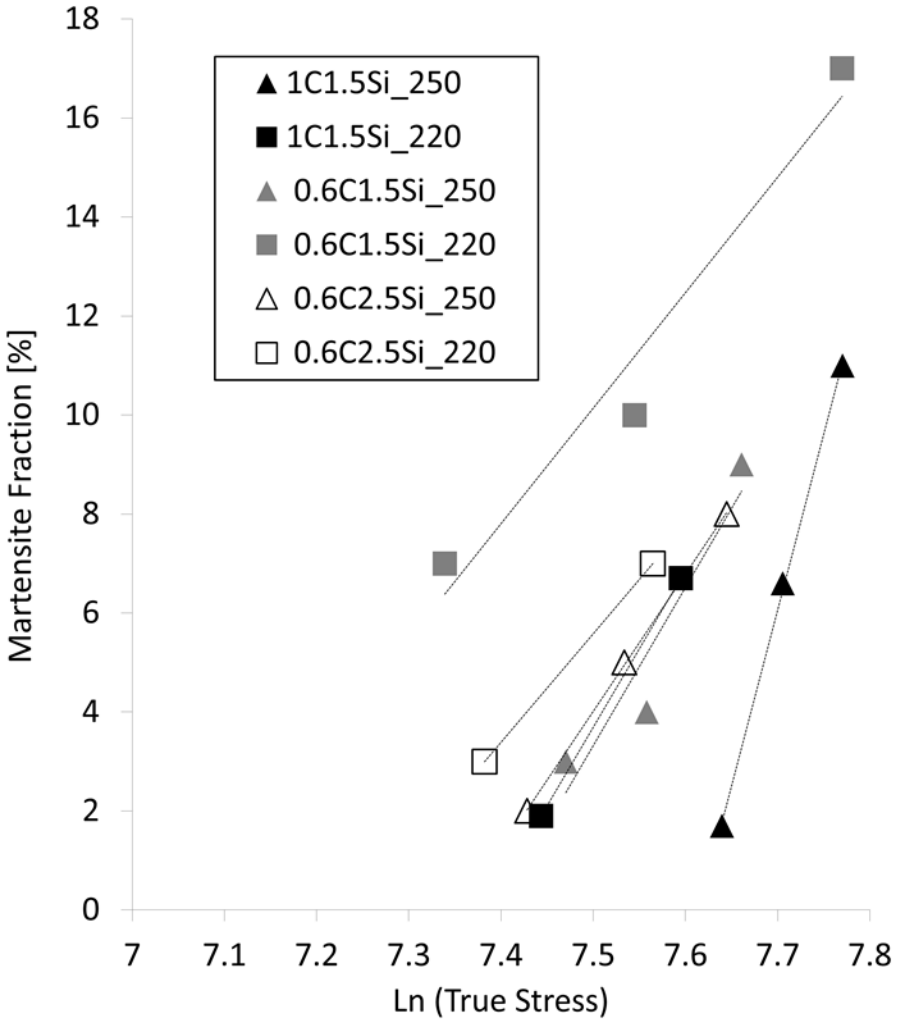

Fig.2. Experimentally obtained fraction of martensite vs. Ln of true stress for different interrupted tensile tests within the uniform plastic regime. Linear regression for each sample is superimposed.

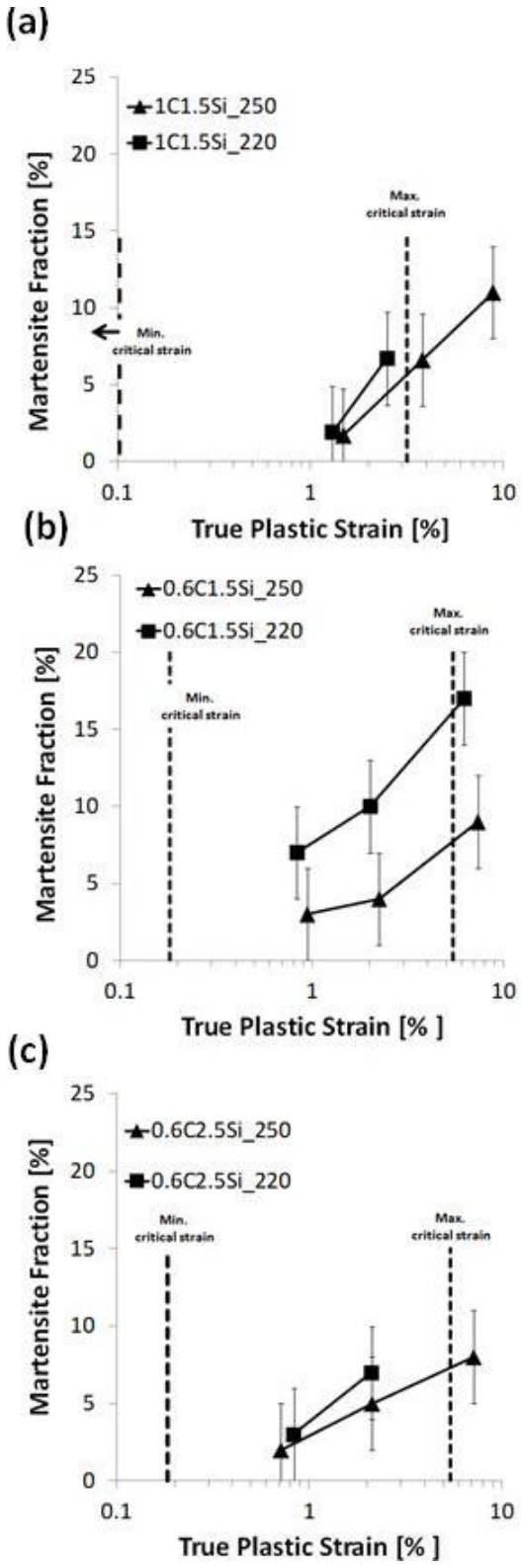

Fig. 3. Experimental data of martensite fraction evolution as a function of the true plastic strain during tensile test. The dotted lines represent the critical strain for martensitic stabilization in two limit cases: min. C content for austenite size of 1μm, and max. C content for austenite size of 50nm.

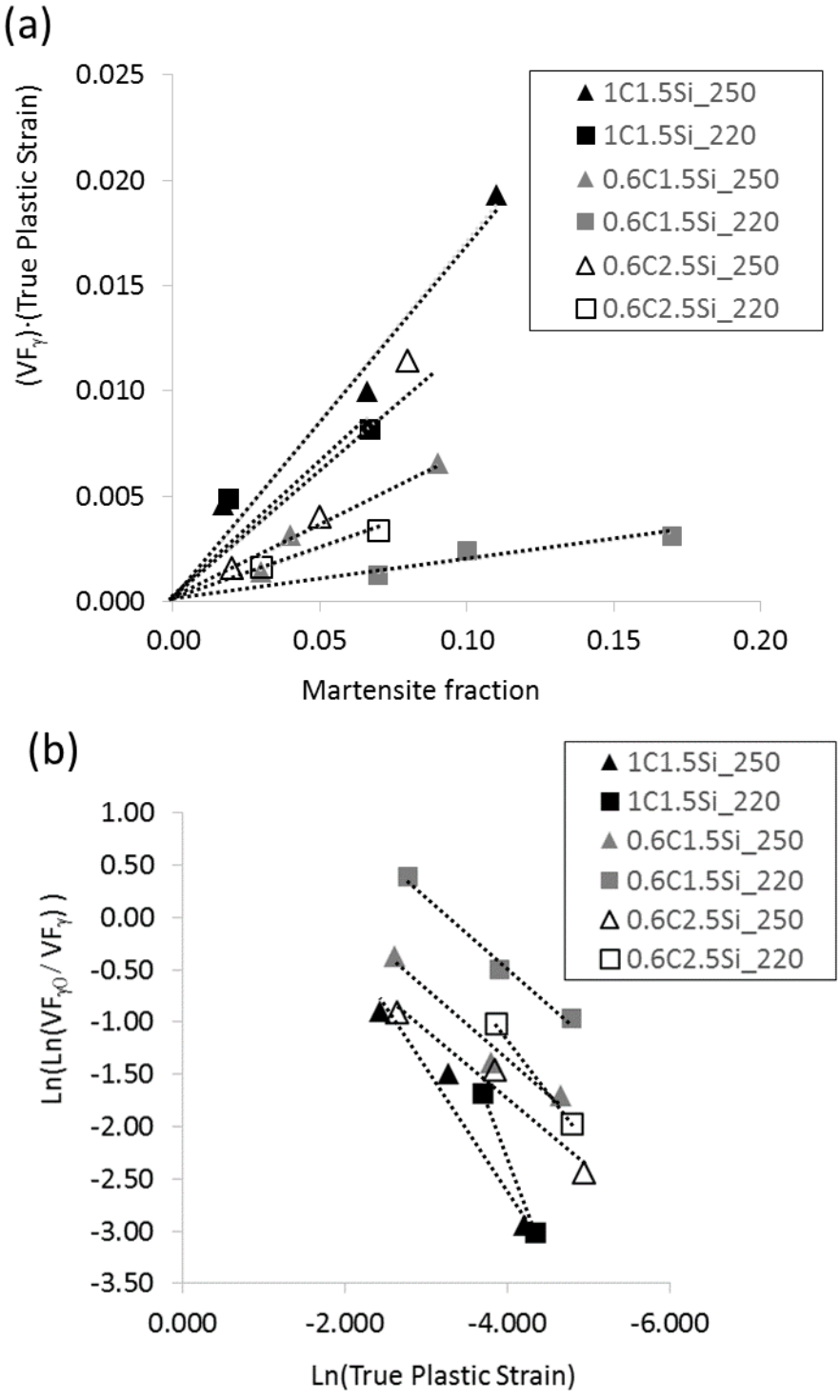

Fig. 4. Strain-assisted matensitic transformation models applied to experimental data: a) BMT model and b) Guimarães model. $VF_{\gamma 0}$ stands for the initial austenite volume fraction and VF_{γ}, for the remaining austenite volume fraction.

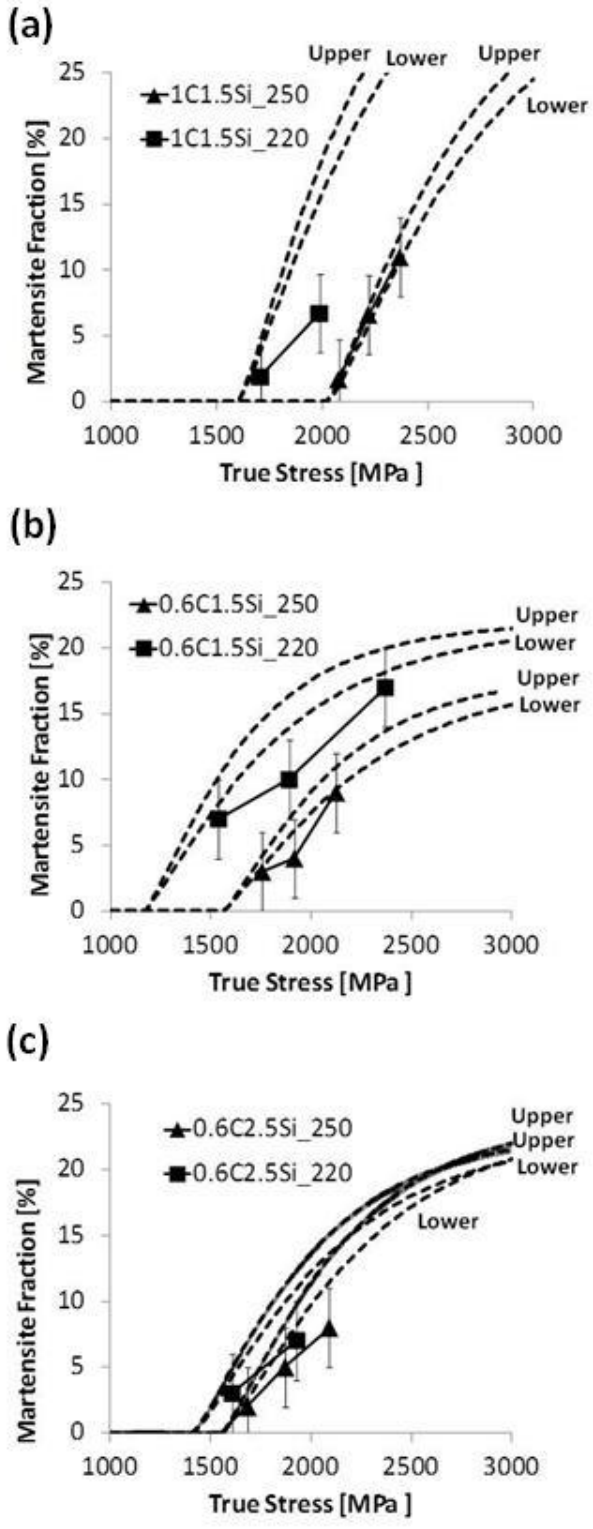

Fig.5. Simulation and experimental data of martensite fraction evolution as a function of the true stress during tensile test. Simulated curves are named with the transformation temperature followed by "upper" or "lower" referring to the austenite C content set as input.

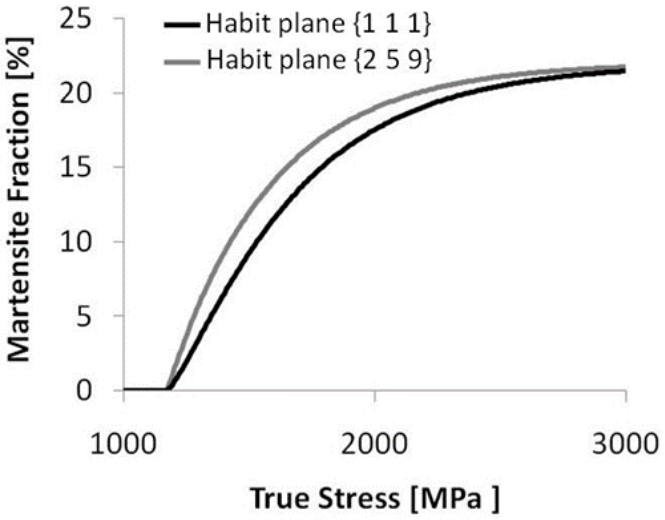

Fig. 6. Comparison between the theoretical austenite evolution as a function of the stress for a habit plane {1 1 1} or {2 5 9}. Inputs are, as an example, those corresponding to Steel 2 treated at 220^{o}C.

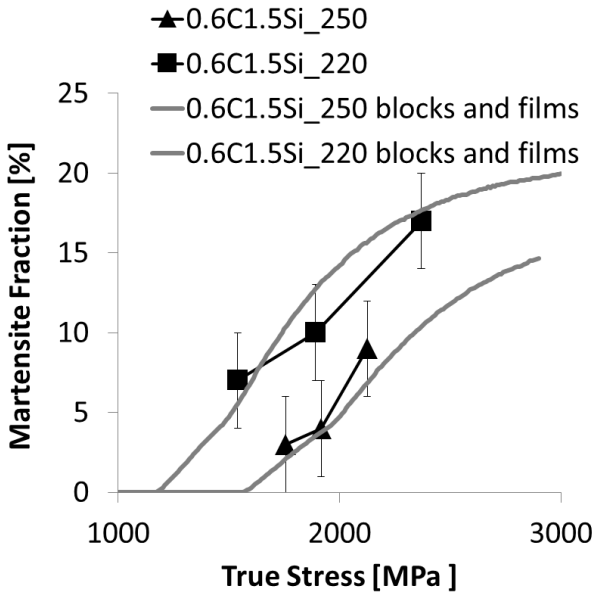

Fig. 7. Simulation and experimental data of martensite fraction evolution as a function of the true stress during tensile test for Steel 2. Simulated curves are generated by an algorithm that considers the presence of austenite blocks and austenite films.

REFERENCES

1P.J. Jacques, E. Girault, Ph. Harlet, F. Delanny, The developments of cold-rolled TRIP-assisted Multiphase steels. Low silicon TRIP-assisted Multiphase steels, ISIJ Int., 41 (2001) 1061-1067.

2 J. Shi, S. Turteltaub, E. Van Der Giessen, Analysis of grain size effects on transformation-induced plasticity based on a discrete dislocation-transformation model, J. Mech. Phys. Solids, 58 (2010) 1863-1878.

3 S. Chatterjee, H. Bhadeshia, Transformation induced plasticity assisted steels: stress or strain affected martensitic transformation, Mater. Sci. Technol., 23 (2007) 1101-1104.

4F. Lani, Q. Furnemont, T. Van Rompaey, F. Delannay, P.J. Jacques, T. Pardoen, Multiscale mechanics of TRIP-assisted multiphase steels: II. Micromechanical modelling, Acta Mater., 55 (2007) 3695-3705.

5 P.J. Jacques, Q. Furnémont, F. Lani, T. Pardoen, F. Delannay, Multiscale mechanics of TRIP-assisted multiphase steels: I. Characterization and mechanical testing, Acta Mater., 55 (2007) 3681-3693.

6 R.G. Stringfellow, D.M. Parks, G.B. Olson, A constitutive model for transformation plasticity accompanying strain-induced martensitic transformations in metastable austenitic steels, Acta Metall. Mater., 40 (1992) 1703-1716.

7 D.D. Tjahjanto, S. Turteltaub, A.S.J. Suiker, S. Van Der Zwaag, Modelling of the effects of grain orientation on transformation-induced plasticity in multiphase carbon steels, Modell. Simul.Mater. Sci. Eng., 14 (2006) 617-636.

8 R. Sierra, J.A. Nemes, Investigation of the mechanical behaviour of multi-phase TRIP steels using finite element methods, Int. J. Mech. Sci., 50 (2008) 649-665.

9M.-G. Lee, S.-J.Kim, H.N. Han, Crystal plasticity finite element modeling of mechanically induced martensitic transformation (MIMT) in metastable austenite, Int. J. Plast., 26 (2010) 688-710.

10 C. Garcia-Mateo, F.G. Caballero, M.K. Miller, J.A. Jimenez, On measurement of carbon content in retained austenite in a nanostructured bainitic steel, J. Mater. Sci., 47 (2012) 1004-1010.

11 Y. Tomota, H. Tokuda, Y. Adachi, M. Wakita, N. Minakawa, A. Moriai, Y. Morii, Tensile behavior of TRIP-aided multi-phase steels studied by in situ neutron diffraction, Acta Mater., 52 (2004) 5737-5745.

12P.J. Jacques, J. Ladrière, F. Delannay, On the influence of interactions between phases on the mechanical stability of retained austenite in transformation-induced plasticity multiphase steels, Metall. Mater. Trans. A, 32 (2001) 2759-2768.

13 P. Wang, N. Xiao, S. Lu, D. Li, Y. Li, Investigation of the mechanical stability of reversed austenite in 13%Cr-4%Ni martensitic stainless steel during the uniaxial tensile test, Mater. Sci. Eng. A, 586 (2013) 292-300.

14 C. Garcia-Mateo, F.G. Caballero, T. Sourmail, M. Kuntz, J. Cornide, V. Smanio, R. Elvira, Tensile behaviour of a nanocrystalline bainitic steel containing 3 wt% silicon, Mater. Sci. Eng. A, 549 (2012) 185-192.

15 C. Garcia-Mateo, F.G. Caballero, The role of retained austenite on tensile properties of steels with bainitic microstructures, Mater. Trans. JIM, 46 (2005) 1839-1846.

16 C.N. Hulme-Smith, I. Lonardelli, A.C. Dippel, H.K.D.H. Bhadeshia, Experimental evidence for non-cubic bainitic ferrite, Scr. Mater., 69 (2013) 409-412.

17 C.N. Hulme-Smith, M.J. Peet, I. Lonardelli, A.C. Dippel, H.K.D.H. Bhadeshia, Further evidence of tetragonality in bainitic ferrite, Mater. Sci. Technol., 31 (2015) 254-256.

18 C. Garcia-Mateo, J.A. Jimenez, H.W. Yen, M.K. Miller, L. Morales-Rivas, M. Kuntz, S.P. Ringer, J.R. Yang, F.G. Caballero, Low temperature bainitic ferrite: Evidence of carbon super-saturation and tetragonality, Acta Mater., 91 (2015) 162-173.

19 ASTM E975-03 Standard Practice for X-Ray Determination of Retained Austenite in Steel with Near Random Crystallographic Orientation, ASTM International, (2008).

20 N.P. Laboratory, MTDATA, Teddington, Middlesex, UK, TW11 0LW, 2003.

21 F. Bachmann, R. Hielscher, H. Schaeben, Texture analysis with MTEX- Free and open source software toolbox, Solid State Phenom., 2010, pp. 63-68.

22 MATLAB (MathWorks, Inc., Natick, MA, USA)

23 E. Kozeschnik, H.K.D.H. Bhadeshia, Influence of silicon on cementite precipitation in steels, Mater. Sci. Technol., 24 (2008) 343-347.

24 C. Garcia-Mateo, H.K.D.H. Bhadeshia, F.G. Caballero, Development of Hard Bainite, ISIJ Int., 43 (2003) 1238-1243.

25 C. Garcia-Mateo, H.K.D.H. Bhadeshia, F.G. Caballero, Acceleration of low-temperature bainite, ISIJ Int., 43 (2003) 1821-1825.

26 H.K.D.H. Bhadeshia, Anomalies in carbon concentration determinations from nanostructured bainite, Mater. Sci. Technol., 31 (2015) 758-763.

27 C. Garcia-Mateo, T. Sourmail, F.G. Caballero, V. Smanio, M. Kuntz, C. Ziegler, A. Leiro, E. Vuorinen, R. Elvira, T. Teeri, Nanostructured steel industrialisation: plausible reality, Mater. Sci. Technol., 30 (2014) 1071-1078.

28 C. Garcia-Mateo, F.G. Caballero, Ultra-high-strength bainitic steels, ISIJ Int., 45 (2005) 1736-1740.

29 S.B. Singh, H.K.D.H. Bhadeshia, Estimation of bainite plate-thickness in low-alloy steels, Mater. Sci. Eng. A, 245 (1998) 72-79.

30 S.S. Babu, S. Vogel, C. Garcia-Mateo, B. Clausen, L. Morales-Rivas, F.G. Caballero, Microstructure evolution during tensile deformation of a nanostructured bainitic steel, Scr. Mater., 69 (2013) 777-780.

31 H.K.D.H. Bhadeshia, The bainite transformation: unresolved issues, Mater. Sci. Eng. A, 273–275 (1999) 58-66.

32 E.S. Machlin, M. Cohen, Burst phenomenon in the martensitic transformation, Trans. Am. Inst. Min. Metall. Eng., 191 (1951) 746-754.

33 G.B. Olson, Morris Cohen: A memorial tribute, Mater. Sci. Eng. A, 438-440 (2006) 2-11.

34 K. Tsuzaki, S. Fukasaku, Y. Tomota, T. Maki, Effect of prior deformation of austenite on the gamma-epsilon martensitic-transformation in Fe-Mn alloys, Mater. Trans., JIM, 32 (1991) 222-228.

35 S. Chatterjee, H.S. Wang, J.R. Yang, H.K.D.H. Bhadeshia, Mechanical stabilisation of austenite. Mater. Sci. Technol. 2006, 22 (6), 641-644.

36 J.C. Bokros, E.R. Parker, The mechanism of the martensite burst transformation in FeNi single crystals, Acta Metall., 11 (1963) 1291-1301.

37 S. Kundu, K. Hase, H.K.D.H. Bhadeshia, Crystallographic texture of stress-affected bainite, Proceedings of the Royal Society A: Mathematical, Physical and Engineering Sciences, 463 (2007) 2309-2328.

38 L. Samek, E. De Moor, J. Penning, B.C. De Cooman, Metall. Mater. Trans. B, 37A (2006) 109-124.

39 J. Burke, in, Pergamon Press, Oxford; New York, 1965.

40 O. Matsumura, Y. Sakuma, H. Takechi, Scr. Metall., 21 (1987) 1301-1306.

41 T.Y. Tsuchida N, Mater. Sci. Eng. A, A285 (2000) 345-352.

42 J.R.C. Guimaraes, Scr. Metall., 6 (1972) 795-798.

43 G.B. Olson, M. Cohen, Metall. Trans. A, A 6 (1975) 791-795.

44 J.H. Ryu, D.-I. Kim, H.S. Kim, H.K.D.H. Bhadeshia, D.-W. Suh, Strain partitioning and mechanical stability of retained austenite, Scr. Mater., 63 (2010) 297-299.

45 S. Kundu, H.K.D.H. Bhadeshia, Transformation texture in deformed stainless steel, Scr. Mater., 55 (2006) 779-781.

46 D.P. Koistinen, R.E. Marburger, A general equation prescribing the extent of the austenite-martensite transformation in pure iron-carbon alloys and plain carbon steels, Acta Metall., 7 (1959) 59-60.

47 H.K.D.H. Bhadeshia, Bainite in Steels, Second ed., Institute of Materials, Maney Publishing, London, 2001.

48 H.K.D.H. Bhadeshia, Worked examples in the geometry of crystals, Second ed., The Institute of Metals North American Publications Center, Brookfield, VT 05036, USA, 2001.

49 J.R. Patel, M. Cohen, Criterion for the action of applied stress in the martensitic transformation, Acta Metall., 1 (1953) 531-538.

50 L. Morales-Rivas, A. González-Orive, C. Garcia-Mateo, A. Hernández-Creus, F. G. Caballero, L. Vázquez, Nanomechanical characterization of nanostructured bainitic steel: Peak Force Microscopy and Nanoindentation with AFM, Scientific Reports | 5:17164 | (2015) DOI: 10.1038/srep17164

51 P.J. Jacques, J. Ladrière, F. Delannay, On the influence of interactions between phases on the mechanical stability of retained austenite in transformation-induced plasticity multiphase steels, Metall. Mater. Trans. A, 32 (2001) 2759-2768.

52 H.F. Lan, X.-H. Liu, L.-X. Du, Ultra-Hard Bainitic Steels Processed through Low Temperature Heat Treatment. Advanced Manufacturing Technology, Pts 1, 2. J.T. Han, Z.Y. Jiang and S. Jiao. 156-157 (2011) 1708-1712.